Available online at http://scik.org

J. Math. Comput. Sci. 10 (2020), No. 4, 1192-1213

https://doi.org/10.28919/jmcs/4587

ISSN: 1927-5307

PERISTALTIC PUMPING IN BUONGIORNO MODEL NANOFLUIDS TRANSPORT WITHIN FLEXIBLE WALLS

BHIMANAND PANDURANG GAJBHARE[1,*], J.S.V.R. KRISHNA PRASAD[2], S.R. MISHRA[3]

[1]Department of Mathematics, Vaidyanath College Parli-Vaijanath, Beed-431515, Maharashtra, India

[2]Department of Mathematics, Moolji Jaitha College, Jalgaon, Maharashtra, India

[3]Department of Mathematics, Siksha 'O' Anusandhan Deemed to be University, Khandagiri Square, Bhubaneswar-751030, Odisha, India

Abstract: Peristaltic pumping is a mechanism always takes place from lower pressure region to higher pressure region. The Buongiorno model nanofluid transport for peristaltic pumping within flexible walls has several many applications such as, urine transport between kidney and bladder, drug delivery in blood vessels etc. Several pharmacological delivery systems including industrial applications are the basic principle of peristaltic pumping in transport systems. In the current research work, Buongiorno model nanofluid is undertaken for the peristaltic pumping within flexible walls. The mechanism through an electrically conducting nanofluid warrants the effect of magnetic field. In addition to that, the influences of thermal radiation, Brownian motion, thermophoresis, and constant heat source/sink are deployed in the present investigation. The simplified nonlinear governing equations are solved numerically and the observations for the embodying parameters are displayed via graphs and tabular form. In particular situation the result shows a conformation with that of earlier investigations warrants carrying forward further investigation and the conclusive remarks are elaborated in the results and discussion section.

Keywords: peristaltic pumping; asymmetric channel; Buongiorno model; radiative heat transfer; Brownian and thermophoresis; numerical solution.

2010 AMS subject classification: 60J65, 85A25

*Corresponding author

E-mail address: bpgajbhare@gmail.com

Received March 19, 2020

1. INTRODUCTION

Peristalsis is the means of transporting liquid through muscle relaxation and an extensible channel or tube contraction. The Peristalsis is the pumping and mixing method of fluid in wave propagation anterograde direction. Gastrointestinal tract, hemolysis, bypass surgery, esophagus, lymph, small intestine and peristaltic pump and heart-lung machines are peristalsis that play a significant role in the transport of physiological liquids and have a enormous amount of biological and biomedical system apps. From Latham's seminal work [1], many studies have been submitted to date on peristaltic flows under different flow geometries and assumptions using analytical methods, numerical techniques and experiments. In latest requirements to enhance the efficiency of prospective emerging technologies such as pharmaceutical procedures,

Nomenclature

c	volumetric volume expansion coefficient	μ	coefficient of viscosity
T_m	fluid mean temperature	ρ_f	fluid density
ρ_p	density of the particle	κ	thermal conductivity
$\hat{\partial}/\hat{\partial}t'$	material time derivative	$\overset{*}{p}$	pressure
T	nanoparticle temperature	C	nanoparticle concentration
D_T	themophoretic diffusion coefficient	q_r	radioactive heat flux
D_B	Brownian diffusion coefficient		
Q_0	constant heat addition/absorption	α	thermal expansion coefficient
β'	expansion with concentration coefficient	σ^*	electrical conductivity
p	dimensionless pressure	R	Reynolds number
a	amplitudes of left wall	b	amplitudes of right wall
Sc	Schmidt number	δ	wave number
ψ	stream function θ dimensionless temperature	Pr	Prandtl number
β	non-dimensional heat source parameter	Gr	Grashof number
M	Hartmann number	Nb	Brownian parameter
Br	local nanoparticle Grashof number	Bi_N	mass Biot number
Bi_T	heat Biot number	Nt	thermophoresis parameter
σ	nanoparticle volume fraction	R_n	thermal radiation parameter.

thermal exchangers, hybrid microelectronics and electric motors, solar collectors in which nanometer-sized solid particles are suspended in the base liquid, few latest papers in this direction are stated in references [2–13]. Water, oil, ethylene glycol, and other lubricants are the common base fluids in nanofluid. Earlier studies have shown that nanoparticle suspension in a base fluid significantly reflects the flow properties and heat transfer features in a standard base fluid. Choi's used original term "nanofluid" [14]. It defines an ultra-fine particle fluid suspension (diameter less than 50 nm). In nonmanufacturing, many cheap combinations of liquid / particle are now available. The natural convective boundary-layer flow of a nanofluid near a vertical plate was analytically explored by Kuznetsov and Nield [15]. They've been using a model. In this model, the Brownian movement and thermophoresis impacts were incorporated. Some of the past nanofluid research [16-17] were provided to evaluate nanofluid heat properties. Buongiorno [18-19] explored a four-component nonhomogeneous balanced model for heat, mass, and momentum in nanofluids. He noted that for the slip scheme of nanoparticles, thermophoresis and Brownian diffusion were the most important, as well as enlightenment for the uneven heat transfer increase ready for nanofluids. Shi et al. [20] explored and numerically simulated the characteristics of natural convection on thermophysical nanofluids Fe3O4@CNT. They also evaluated how magnetic field impacts can alter heat transfer efficiency. There has been extensive discussion of the issue of nanofluid flow and thermal transfer [21-22]. In a wide range of magnetic recording media, magnetic resonance contrast media, and biomedical applications, magnetic nanoparticles play one of the most significant roles and have great potential for investigations. Each magnetic nanoparticle has different properties, e.g., magnet and optical properties of synthesized iron nanoclusters [23], ferrimagnetic magnetite powders produced by arc-discharge system in a partial oxygen atmosphere [24], enormous room temperature magnetoresistance synthetic surface Fe nanoclusters on SiO_2 [25], permeable powders made by arc-discharge scheme with 78 % or 45% synthetic surface Fe. Due to their best quality heat characteristics, nanoscale particles are now engaged in the solar energy system. It is also very useful to plan innovative products such as photocatalysts, low concentration organic contaminants, electrical energy production and environmental restoration, and because of its powerful oxidizing strength and long-term stability [26-27]. Zeiny et al. [28] addressed solar thermal conversion efficiency based hybrid nanofluids and also studied photothermal conversion efficiency (PTE) through the law of Beer. They extracted price of the optical properties of

nanofluids used to estimate the theoretical PTE, absorption rate, and equipment. Recently, scientists have focused their job on nanofluids that rely on nanoparticles with elevated thermal conductivity to increase the heat transfer rate efficiency and their heat transfer can be regulated by the magnetic field. Shi et al.[29], which combines the characteristics of Fe_3O_4 and TiO_2 nanoparticles to provide a recyclable purification and separation, presents the efficient strategy for convenient synthesizing $Fe_3O_4@TiO_2$ nanoparticles. They also likened the detachment of the nanoparticles $Fe_3O_4@TiO_2$ at the magnetic field's different magnitude. Prakash et al. [30] lately created the mathematical model of solar peristaltic nanofluid MHD micro-pump in which nanofluid viscosity, thermal radiation, source / sink heat and water permeability impacts were regarded. Akram et al. [31] researched the peristaltic transport of nanofluids in asymmetric walls. Heidary and Kermani [32] are numerically calculated the flow field and heat transfer analysis in flexible walls. Nadeem and Akbar [33] have researched the peristaltic transport of a nanofluid in an endoscope.

Owing to the past knowledge, present study reveals the MHD nanofluid transport using peristaltic pumping in an asymmetric channel. The model based on the Buongirnio nanofluid model for the interaction of Brownian motion and thermophoresis parameters of the transport phenomena. Emphasis goes on the heat and mass flux boundary conditions involving with Biot numbers for both temperature and nanoparticles. Simulation of the parameters at the time of numerical solution is obtained using the mathematical software MATLAB with in-build code bvp4c. Moreover, computation is carried out with an average CPU time 0.1346 for each.

2. FORMALISM OF THE PROPOSED MODEL

Nanofluid transport of peristaltic fluid based on Buongiorno model within fixed walls has been considered. Both the wall is placed at fixed width $2d$. The proposed model brings out the influence of both Brownian motion and thermophoresis on the temperature and solutal concentration profiles. Energy equation is enhanced with incorporating the thermal radiation and constant heat source/sink. The influence of solutal reactant is used to enhance the nanoparticle concentration. Under the action of transverse magnetic field of strength B_0 , is applied normal to the flow direction. Nanoparticle volume fraction within the asymmetric channel is used to predict the heat exchanges and convective mass transfer. The rectangular coordinates system for the channel where $\overset{*}{\xi}$ is parallel to the middle channel and $\overset{*}{\eta}$ is transverse to the flow field (fig.1).

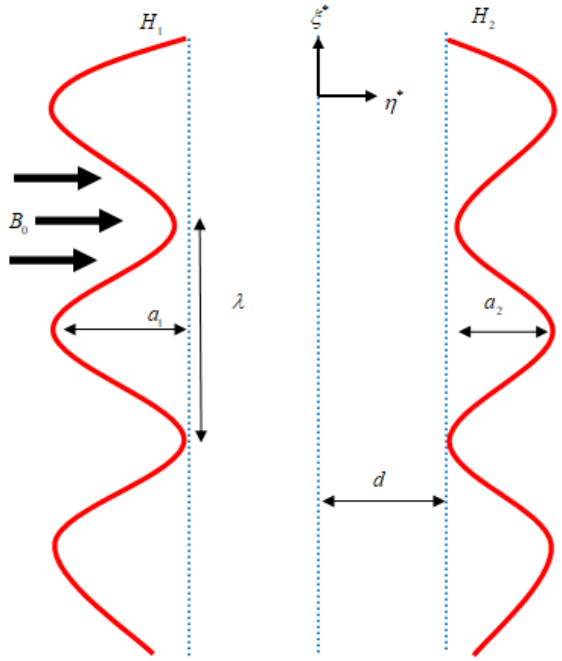

Fig. 1 geometrical configuration

The formulated equations with their boundary conditions are as follows

$$\frac{\partial \overset{*}{u}}{\partial \overset{*}{\xi}} + \frac{\partial \overset{*}{v}}{\partial \overset{*}{\eta}} = 0 \tag{1}$$

$$\rho_f \left(\frac{\partial}{\partial t'} + \overset{*}{u}\frac{\partial}{\partial \overset{*}{\xi}} + \overset{*}{v}\frac{\partial}{\partial \overset{*}{\eta}} \right) \overset{*}{u} = -\frac{\partial \overset{*}{p}}{\partial \overset{*}{\xi}} + \mu \left[\frac{\partial^2 \overset{*}{u}}{\partial \overset{*2}{\xi}} + \frac{\partial^2 \overset{*}{u}}{\partial \overset{*2}{\eta}} \right] - \sigma^* B_0^2 \overset{*}{u} + \left(\rho_p - \rho_f \right) \beta' g \left(C - C_0 \right) + \left(1 - C_0 \right) \rho_f \alpha g \left(T - T_0 \right) \tag{2}$$

$$\rho_f \left(\frac{\partial}{\partial t'} + \overset{*}{u}\frac{\partial}{\partial \overset{*}{\xi}} + \overset{*}{v}\frac{\partial}{\partial \overset{*}{\eta}} \right) \overset{*}{u} = -\frac{\partial \overset{*}{p}}{\partial \overset{*}{\xi}} + \mu \left[\frac{\partial^2 \overset{*}{v}}{\partial \overset{*2}{\xi}} + \frac{\partial^2 \overset{*}{v}}{\partial \overset{*2}{\eta}} \right] \tag{3}$$

$$(\rho c)_f \left(\frac{\partial}{\partial t'} + \overset{*}{u}\frac{\partial}{\partial \overset{*}{\xi}} + \overset{*}{v}\frac{\partial}{\partial \overset{*}{\eta}} \right) T = \kappa \left[\frac{\partial^2 \overset{*}{u}}{\partial \overset{*2}{\xi}} + \frac{\partial^2 \overset{*}{u}}{\partial \overset{*2}{\eta}} \right] + (\rho c)_p \left[D_B \frac{\partial C}{\partial \overset{*}{\xi}} \frac{\partial T}{\partial \overset{*}{\xi}} + \frac{\partial C}{\partial \overset{*}{\eta}} \frac{\partial T}{\partial \overset{*}{\eta}} \right] - \frac{\partial q_r}{\partial \overset{*}{\eta}} + Q_0 + \frac{D_T}{T_m} \left[\left(\frac{\partial T}{\partial \overset{*}{\xi}} \right)^2 + \left(\frac{\partial T}{\partial \overset{*}{\eta}} \right)^2 \right] \tag{4}$$

$$\left(\frac{\partial}{\partial t'}+\overset{*}{u}\frac{\partial}{\partial \overset{*}{\xi}}+\overset{*}{v}\frac{\partial}{\partial \overset{*}{\eta}}\right)C=D_B\left[\frac{\partial^2 C}{\partial \overset{*}{\xi}^2}+\frac{\partial^2 C}{\partial \overset{*}{\eta}^2}\right]+\frac{D_T}{T_m}\left[\frac{\partial^2 T}{\partial \overset{*}{\xi}^2}+\frac{\partial^2 T}{\partial \overset{*}{\eta}^2}\right] \tag{5}$$

$$-k_h\frac{\partial T}{\partial \overset{*}{\eta}}=h_h(T_0-T) \text{ and } -k_m\frac{\partial C}{\partial \overset{*}{\eta}}=h_m(C_0-C) \text{ at } \overset{*}{\eta}=H_1 \tag{6}$$

$$-k_h\frac{\partial T}{\partial \overset{*}{\eta}}=h_h(T-T_1) \text{ and } -k_m\frac{\partial C}{\partial \overset{*}{\eta}}=h_m(C-C_1) \text{ at } \overset{*}{\eta}=H_2 \tag{7}$$

Where h_m and h_h, k_m and k_h are the transport coefficient and conductivity coefficients of both thermal and solutal profiles respectively. The temperature and nanoparticle volume fraction at both the left and right walls are T_0, T_1 and C_0, C_1 respectively and

$$H_1\left(\overset{*}{\xi},t\right)=-d-a_1\cos^2\left[\frac{\pi}{\lambda}(\overset{*}{\xi}-c't)+\phi\right],\ H_2\left(\overset{*}{\xi},t\right)=d+a_2\cos^2\left[\frac{\pi}{\lambda}(\overset{*}{\xi}-c't)\right] \tag{8}$$

Where the amplitudes near the left and right walls are a_1 and a_2 respectively, d is the channel half-width, c' is the wave speed, λ is the wave-length, ϕ is phase difference occurs within an interval $[0,\pi]$.

Imposing the Rosseland approximation $q_r=-\frac{16\sigma'}{3k'}\frac{\partial T}{\partial \overset{*}{\eta}}$ in the heat transfer equation (4) is transformed to

$$\begin{aligned}(\rho c)_f\left(\frac{\partial}{\partial t'}+\overset{*}{u}\frac{\partial}{\partial \overset{*}{\xi}}+\overset{*}{v}\frac{\partial}{\partial \overset{*}{\eta}}\right)T=\kappa\left[\frac{\partial^2 \overset{*}{u}}{\partial \overset{*}{\xi}^2}+\frac{\partial^2 \overset{*}{u}}{\partial \overset{*}{\eta}^2}\right]+(\rho c)_p\left[D_B\frac{\partial C}{\partial \overset{*}{\xi}}\frac{\partial T}{\partial \overset{*}{\xi}}+\frac{\partial C}{\partial \overset{*}{\eta}}\frac{\partial T}{\partial \overset{*}{\eta}}\right]\\ -\frac{\partial}{\partial \overset{*}{\eta}}\left(-\frac{16\sigma'}{3k'}\frac{\partial T}{\partial \overset{*}{\eta}}\right)+Q_0+\frac{D_T}{T_m}\left[\left(\frac{\partial T}{\partial \overset{*}{\xi}}\right)^2+\left(\frac{\partial T}{\partial \overset{*}{\eta}}\right)^2\right]\end{aligned} \tag{9}$$

Following non-dimensional quantities are made use of equations. [1–8],

$$\left.\begin{aligned}
&\xi=\frac{\overset{*}{\xi}}{\lambda},\eta=\frac{\overset{*}{\eta}}{d},t=\frac{c't'}{\lambda},u=\frac{\overset{*}{u}}{c'},v=\frac{\overset{*}{v}}{c'},\delta=\frac{d}{\lambda},h_1=\frac{H_1}{d},h_2=\frac{H_2}{d},\theta=\frac{T-T_0}{T_1-T_0},a=\frac{a_1}{d},\\
&b=\frac{a_2}{d},\sigma=\frac{C-C_0}{C_1-C_0},R=\frac{\rho_f c'd}{\mu},Gr=\frac{(1-C_0)\rho_f g\alpha d^2(T_1-T_0)}{c'\mu},\beta=\frac{Q_0 d^2}{(T_1-T_0)\nu c_p},\\
&\Pr=\frac{\mu c_p}{\kappa},Nb=\frac{\tau D_B(C_1-C_0)}{\nu},Nt=\frac{\tau D_T(C_1-C_0)}{T_0\nu},M=\sqrt{\frac{\sigma^*}{\mu}}dB_0,Rn=\frac{16\sigma' T_0^3}{3k'\mu c_p},Sc=\frac{\nu}{D_B},\\
&Br=\frac{\left(\rho_p-\rho_f\right)g\beta' d^2\left(C_1-C_0\right)}{c'\mu},p=\frac{d^2 p}{c'\lambda\mu},Bi_T=\frac{h_h d}{k_h},Bi_N=\frac{h_m d}{k_m},u=\frac{\partial\psi}{\partial y},v=-\delta\frac{\partial\psi}{\partial y}
\end{aligned}\right\}\quad(10)$$

Further, the non-dimensional form of these equation considering the long wavelength and low Reynolds number are expressed as

$$\frac{\partial p}{\partial\xi}=\frac{\partial^3\psi}{\partial\eta^3}-M^2\frac{\partial\psi}{\partial\eta}+Gr\theta+Br\sigma,\qquad(11)$$

$$\frac{\partial p}{\partial\eta}=0,\qquad(12)$$

$$\left(\frac{1+R_n\Pr}{\Pr}\right)\frac{\partial^2\theta}{\partial\eta^2}+Nb\left(\frac{\partial\sigma}{\partial\eta}\frac{\partial\theta}{\partial\eta}\right)+Nt\left(\frac{\partial\theta}{\partial\eta}\right)^2+\beta=0,\qquad(13)$$

$$\frac{\partial^2\sigma}{\partial\eta^2}+\frac{Nt}{Nb}\frac{\partial^2\theta}{\partial\eta^2}=0\qquad(14)$$

Eliminating pressure gradients from equations (11)-(12), we get

$$\frac{\partial^4\psi}{\partial\eta^4}-M^2\frac{\partial^2\psi}{\partial\eta^2}+Gr\frac{\partial\theta}{\partial\eta}+Br\frac{\partial\sigma}{\partial\eta}=0$$

The boundary conditions in equations (6) and (7) are also transformed to following structure

$$\left.\begin{aligned}
&\psi=\frac{-F}{2},\ \frac{\partial\psi}{\partial\eta}=0,\ \frac{\partial\theta}{\partial\eta}=Bi_T\theta,\qquad\frac{\partial\sigma}{\partial\eta}=Bi_N\sigma,\qquad at\ y=h_1=-1-a\cos^2(\pi(\xi-t)+\phi),\\
&\psi=\frac{-F}{2},\ \frac{\partial\psi}{\partial\eta}=0,\ \frac{\partial\theta}{\partial\eta}=Bi_T(1-\theta),\ \frac{\partial\sigma}{\partial\eta}=Bi_N(1-\sigma),\quad at\ y=h_2=1+b\cos^2(\pi(\xi-t))
\end{aligned}\right\}\quad(15)$$

Following Kikuchi [34], the time rate of blood flow which is an experimental observation defined as $F=\Theta e^{-\varpi t}$, with constants Θ and ϖ. The negative sign indicates the retrograde pumping flow rate, since the peristaltic motion of the flow is deviating the direction of the flow. When volumetric flow rate and pressure rise are both positive then it is denoted as non-negative pumping. Moreover, after the elimination of pressure gradient the entire governing equations and

the boundary conditions are ordinary in nature. Therefore, numerical investigation is performed using Runge-Kutta fourth order method framed in the mathematical software MATLAB with a suitable code bvp4c.

3. RESULTS AND DISCUSSION

Peristaltic flow of Nanofluid based on the Buongiorno model is considered in the present analysis. The flow past an asymmetric fixed wall placed at a distance $2d$ apart, which is fixed. The governing equation becomes coupled due to the interaction of Brownian motion and thermophoresis parameters. In addition to that, thermal radiation is also affecting the transport phenomena. The transformed equations are solved numerically due to the complexity in nature. The behavior of the characterizing parameters is established in the form of graphs, that is, figs. 2-16 and numerical computations are presented via Table-1.Throughout the discussion, the values of the following parameters are fixed except in the particular graph, the variation of the parameters is displayed in the corresponding figures.

3.1 Velocity distributions for various parameters

The influences of magnetic parameter, thermal and nanoparticle Grashof number, and the exponential coefficient on the velocity profiles are displayed in figs. 2-5, for above mentioned fixed values of other characterizing parameters. Fig. 2 describes the effect of magnetic parameter on the velocity profiles of peristaltic blood flow. Symmetric nature in the flow domain is marked from the center of the channel. However, point of inflection between the profiles is observed in the several regions such as $\eta = -0.5$ and $\eta = 0.5$. From these points, the deflection in the profiles is rendered within the channel. In the middle of the channel ($-0.5 < \eta < 0.5$), with an increase in magnetic parameter, the axial velocity profile decreases. Moreover, in the rest of the regions, that is, $\eta > 0.5$ (near to the right wall) and $\eta < -0.5$ (near to the left wall) an increase in magnetic parameter leads to retards the thickness of the channel towards both the walls. The reason is, the magnetic field provides resistance to the fluid flow leads to produce Lorentz force, which has a tendency to slow down the axial velocity as a result fluid motion retards. The comparison with earlier study of Akbar and Nadeem [33] is obtained particularly in the absence of magnetic parameter ($M = 0$), which shows a conformity of the present solution. Also, it is clear to see that the axial velocity attains its maximum value at the centre of the channel. Fig.3 exhibits, the influence of thermal Grashof number on the velocity distribution. Slide tiled towards right of the

channel wall in the profile is marked for several values of the parameter. It is observed that, within the region $\eta < 0$, with an increasing Gr the velocity profile retards however, afterwards, it enhances the velocity profiles. From the middle of the channel, the effect shows reversed in nature. Hike in the velocity profile is marked up to the central region and then falls. The characteristics are quite similar for the influence of nanoparticle Grashof number displayed in fig.4. But the variation is not significant as compared to thermal Grashof number. More precisely, it is clear to validate the present case in the absence of both the Grashof numbers. The characteristic of the constant coefficient ω on the axial velocity is shown fig.5. The mathematical expression used for the velocity boundary condition appears with the coefficient, and it is straight forward that, the exponential function falls rapidly with increasing ω. Therefore, similar characteristic is centered round for the variation of ω on the axial velocity profiles.

3.2 Temperature distribution

Peristaltic transport connected with the phenomenon of mechanical pumping for which we can't avoid the behavior of heat transfer properties associated with various physical parameters. Fig. 6-10 depicts the characteristics of heat source/sink, thermal radiation, Biot number associated with heat transfer, thermophoresis and Brownian motion parameters, respectively. Fig. 6 presents, the influence of heat generation/absorption parameter on the temperature profiles of peristaltic fluid. From equation (13), it is observed that, in the absence of heat source/sink parameter ($\beta = 0$), the equation becomes homogeneous in nature, shows a linear characteristic. In the absence of the parameter, the profile is linear and further, with an increase in heat source the profile increases. Absence of thermal radiation, coincides with the work of Akbar and Nadeem [33], displayed in fig.7. Moreover, an increase in thermal radiation opposes the fluid temperature to enhance. It is because, heat absorption occurs due to the inclusion of thermal radiation, and the heat radiated from heated wall releases more heat energy, as a result, the axial velocity increases but the temperature profile retards throughout the channel. Convective boundary condition is considered for heat flux, causes the interaction of Biot number for heat transport phenomenon, which is presented in fig. 8. Continuous growth in the temperature profile exhibited throughout the channel and maximum growth is observed near the central region. However, increasing Biot number retards the fluid temperature. From the mathematical expression it is clear that, as Biot number increases the thermal conductivity

decreases, as well, resulting decrease in the fluid temperature. The hike in the profile is due to the increase in width of the channel. The influence of thermophoresis (Nt) on the temperature profiles is depicted in fig. 9. Interaction of the terms $Nt\left(\partial\theta/\partial\eta\right)^2$ from equation (13) and $\frac{Nt}{Nb}\frac{\partial^2\theta}{\partial\eta^2}$ from equation (14) causes the behavior of the thermophoresis parameter. Microscopic convection of nanofluid pattern is exhibited in this particular form as presented by Zueco et al.[35]. It is observed that, the fluid temperature enhanced due to an increase in thermophoresis parameter. It is seen that, near the periphery of the channel the flow regime seems to be cool for which the temperature depresses. The migration of the nanoparticles with the thermophoresis along the direction of temperature gradient has a prominent effect for the enhancement of the fluid temperature within the channel. Fig.10 portrays the behavior of the Brownian motion on the fluid temperature. From equations (13) and (14), the terms containing the mixed derivative, $Nb\frac{\partial\theta}{\partial\eta}\frac{\partial\phi}{\partial\eta}$ and higher order derivative term $\frac{Nt}{Nb}\frac{\partial^2\theta}{\partial\eta^2}$, respectively represent the appearance of Brownian motion. Similar trend in the profile is marked as described for thermophoresis, but the picture of the profile is not much significant as thermophoresis parameters. From the initial wall, the growth is also uniform throughout the channel.

3.3 Nanoparticle concentration profiles

Volume fraction plays a vital role on the peristaltic pumping of nanofluid within the channel. Figs.11-16 presents the behavior of various physical parameters on the concentration profiles. Fig.11 presents, the behavior of heat source on the concentration profiles for the fixed values of other pertinent parameters. Concentration profile decelerates with increasing values of the heat source parameters. Moreover, near the left wall, that is, periphery of the channel, the trend showing backward in nature up to the middle of the channel and afterwards, it overshoots the profile. It is observed that, higher concentration is desired towards the right wall. Fig.12 displays, the variation of thermal on the volume fraction / concentration profiles. Rapid growth is marked within the channel from the region $\eta > 0.2$ with an increase in thermal radiation, but for $\eta < 0.2$ slight deceleration in the profiles is marked. The increase in the profile is tangential in nature. The fact is due to the conjunction of radiation with nanoparticle volume fraction causes absorption of radiated heat, for which more heat energy is produced in the fluid regime, resulted in the profile increases. Nanoparticle Biot number also favourable to enhance the fluid

concentration within the channel as shown in the fig.13. The appearance of Biot number is due to the consideration of convective boundary condition, that is, the mass flux condition. From the mathematical expression of the boundary conditions at both the walls, it is clear that, in the right wall the diffusion is comparatively less than that of the left wall, for which their is an increase in Biot number, the hike is maximum near the right wall as compared to the periphery of the channel. Fig.14 exhibits the influence of thermophoresis parameter on the concentration profiles. In the aabsence of thermophoresis, the concentration level is more throughout the channel; however, retardation in the profile is marked as increase in the thermophoresis. But two layered variation is marked for the variation of Brownian motion parameter as displayed in the fig.15. For the low value of Brownian motion, the profile also lower down and showing its linear characteristics. However, for the higher values, the rate of concentration increases rapidly within the flow regime.

3.4 Numerical result for the variation of time period

Finally, computed values of both, the primary velocity as well as axial velocity in the fluid regime for various times are obtained and presented in Table- 1. It is observed that, in both, the absence and presence of time period *t*, the primary velocity varies from negative domain to positive, whereas the axial velocity showing its symmetric behavior about the central region of the channel.

4. CONCLUDING REMARKS

The current study deals with the analysis of Brownian motion and thermophoretic parameter on the electromagnetic flow of nanofluid based upon Buongiorno model aggravated by peristaltic pumping. Influences of thermal radiation, constant heat source and chemical reaction enrich the subject as well. Approximate solutions for the highly nonlinear coupled governing equations are obtained employing Runge-Kutta fourth order method. Behavior of the characterizing parameters embodiedd with the flow phenomena are obtained and discussed. The extraction of some important outcomes are laid down.

- Validation with earlier studies is a road map to the further analysis of the present problem.
- Axial velocity break down to three different regions due to the variation of magnetic parameter showing the usual retardation in the axial velocity profiles.

- Enhancement of constant heat source boosts the fluid temperature within the channel.
- Both the thermophoresis and Brownian motion parameter come forward to reduce the channel thickness near the periphery of the channel.
- Biot number caused due to heat transport decelerates the fluid temperature, whereas, the Biot number formed due to solutal transport favors to enhance the fluid concentration.
- An increase in time period along with channel width enhances the primary velocity distributions.

Last but not least, the present investigation on the phenomenon of peristaltic pumping is a physiological study for the blood flow in the artery, which can be helpful to the society in various aspects. However, there is a lot of scope to extend the research work in future.

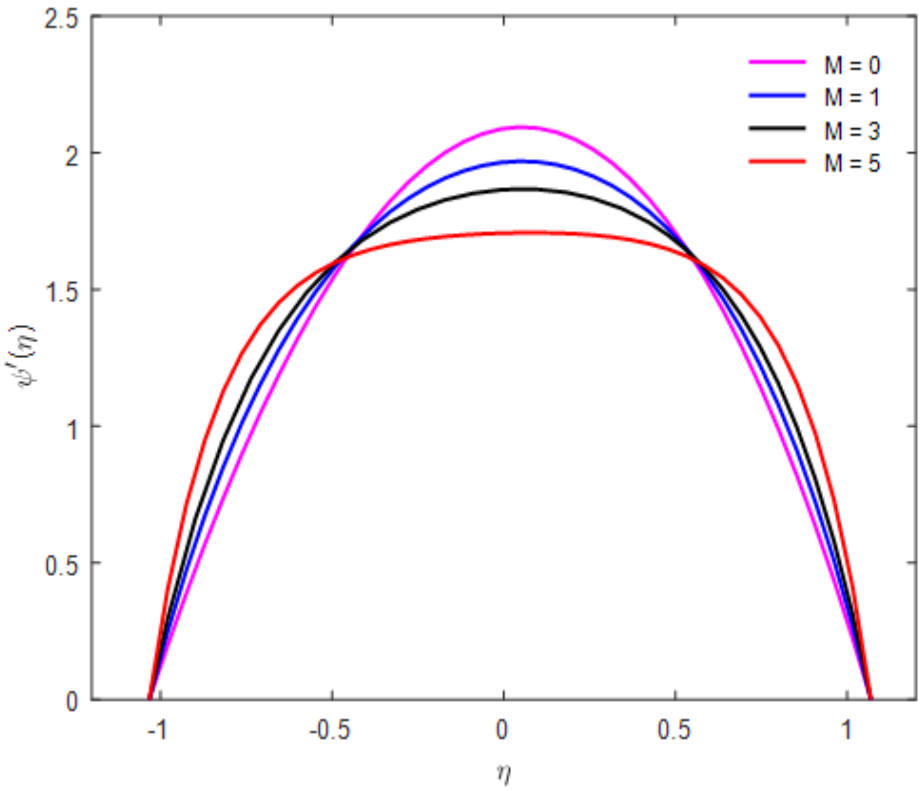

Fig.2 Variation of M on axial velocity

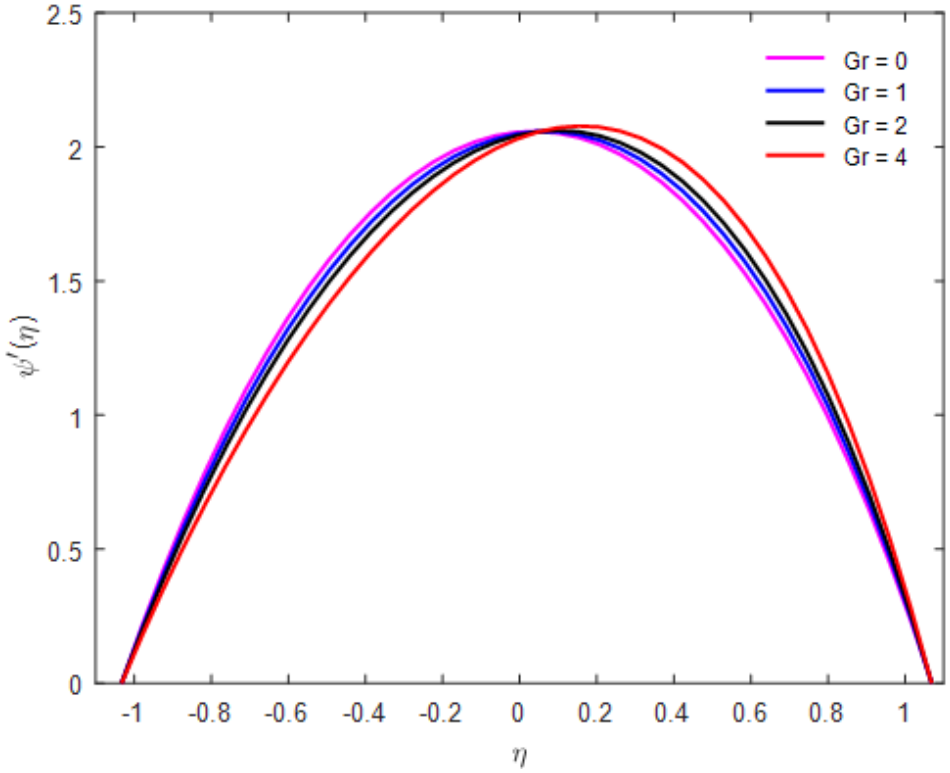

Fig.3 Variation of Gr on axial velocity

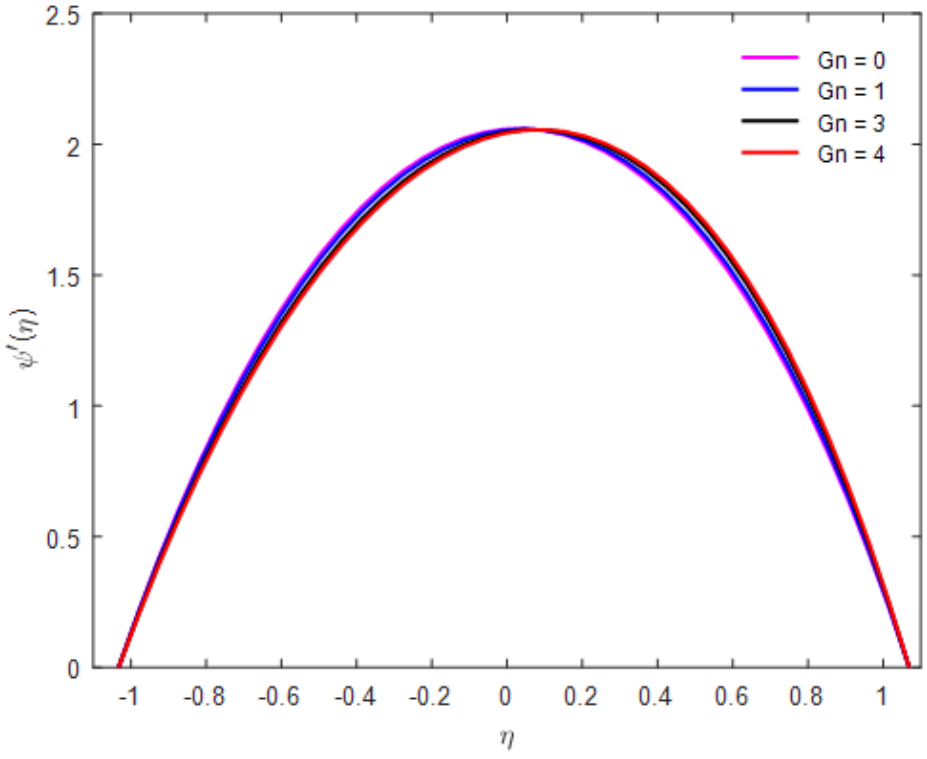

Fig.4 Variation of Gn on axial velocity

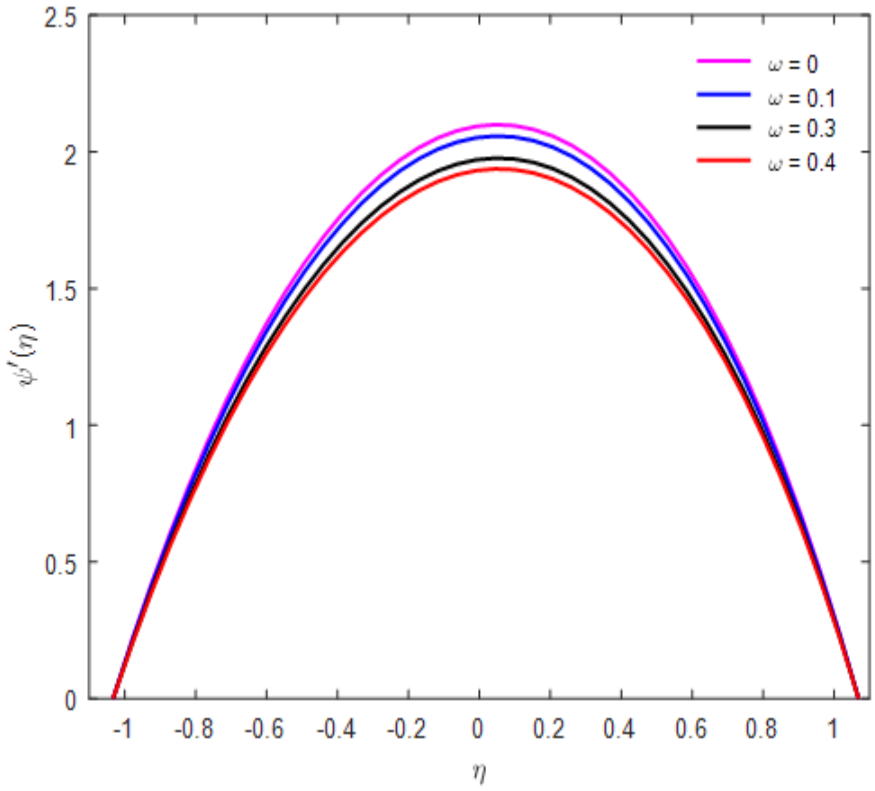

Fig.5 Variation of ω on axial velocity

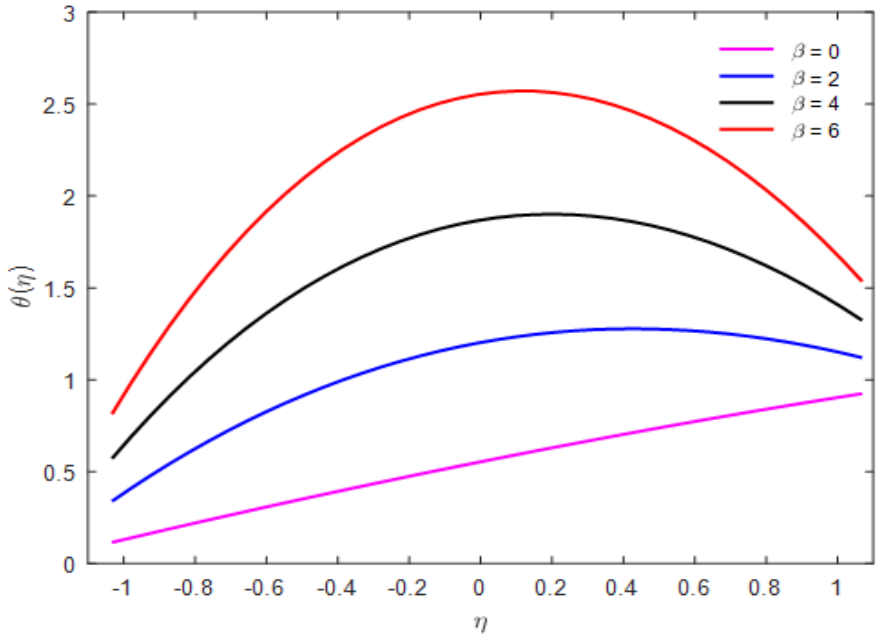

Fig.6 Variation of β on fluid temperature

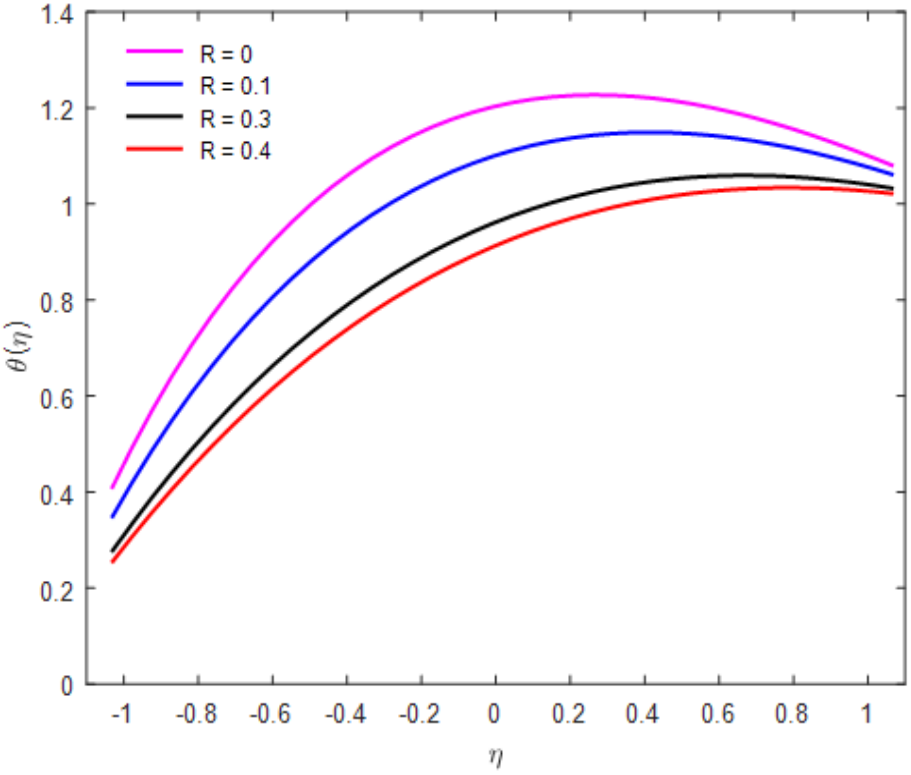

Fig.7 Variation of R on fluid temperature

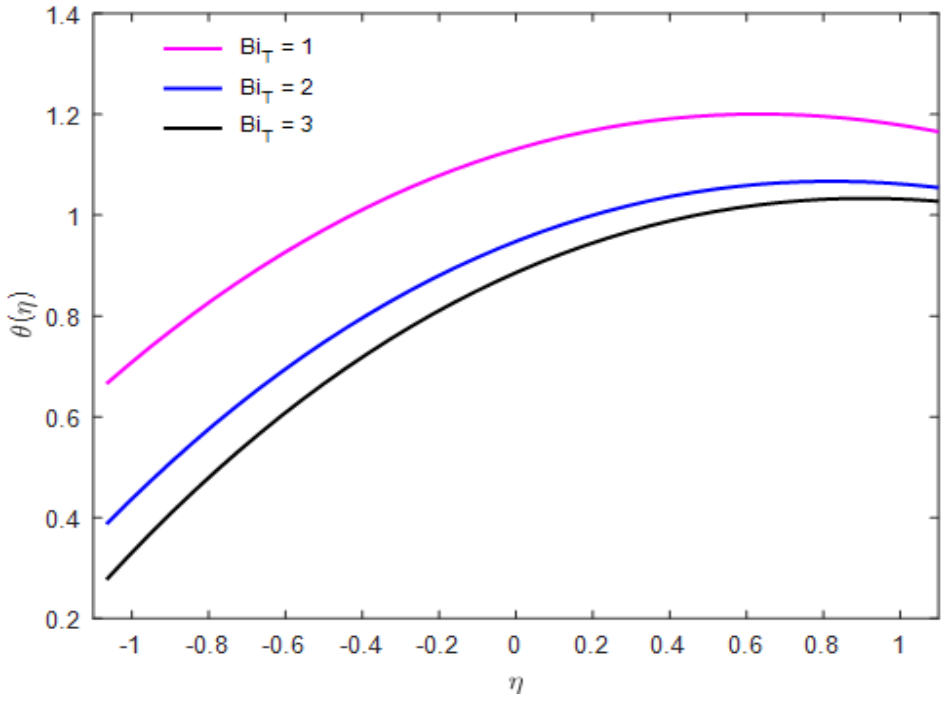

Fig.8 Variation of Bi_T on fluid temperature

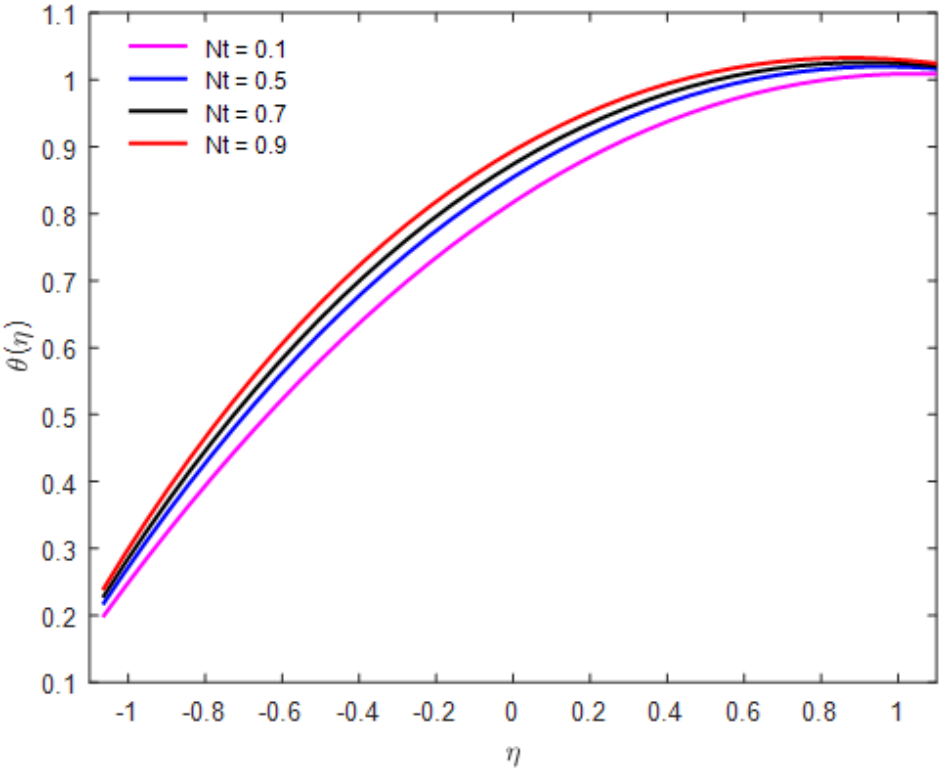

Fig.9 Variation of Nt on fluid temperature

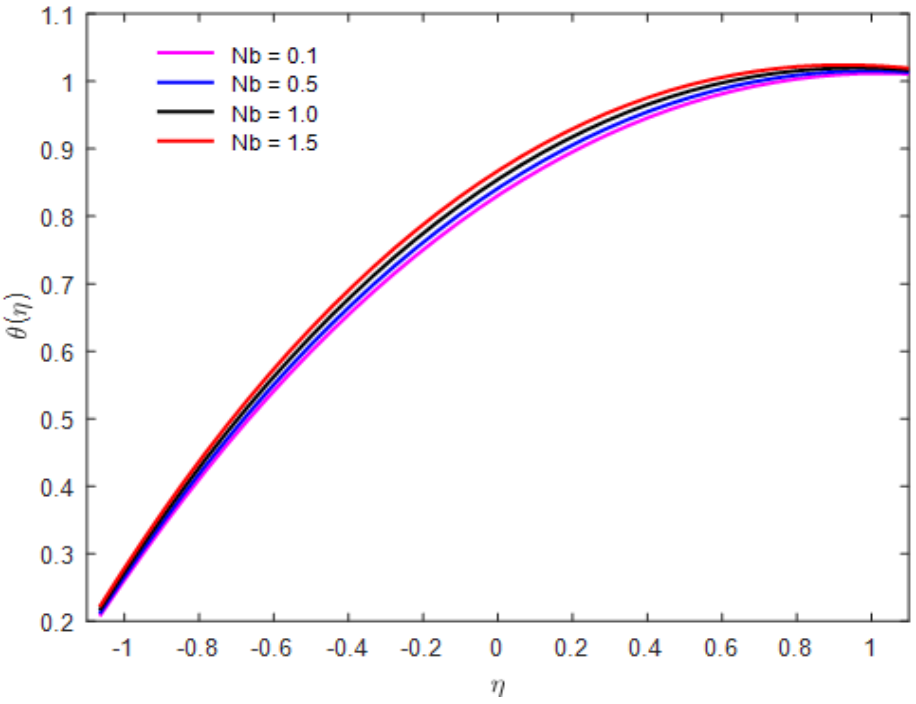

Fig.10 Variation of Nb on fluid temperature

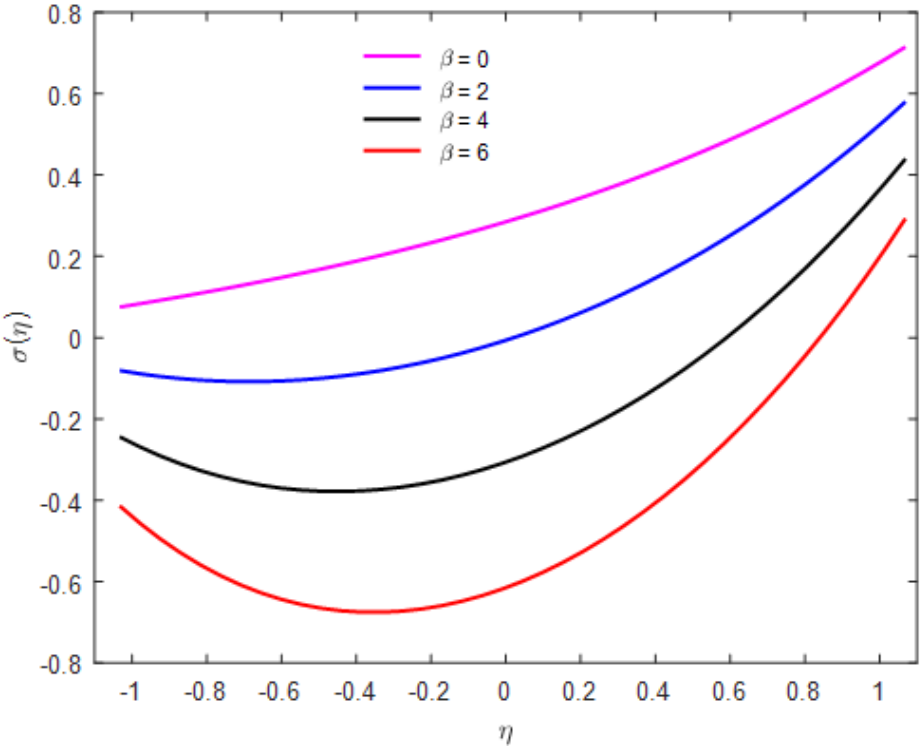

Fig.11 Variation of β on fluid concentration

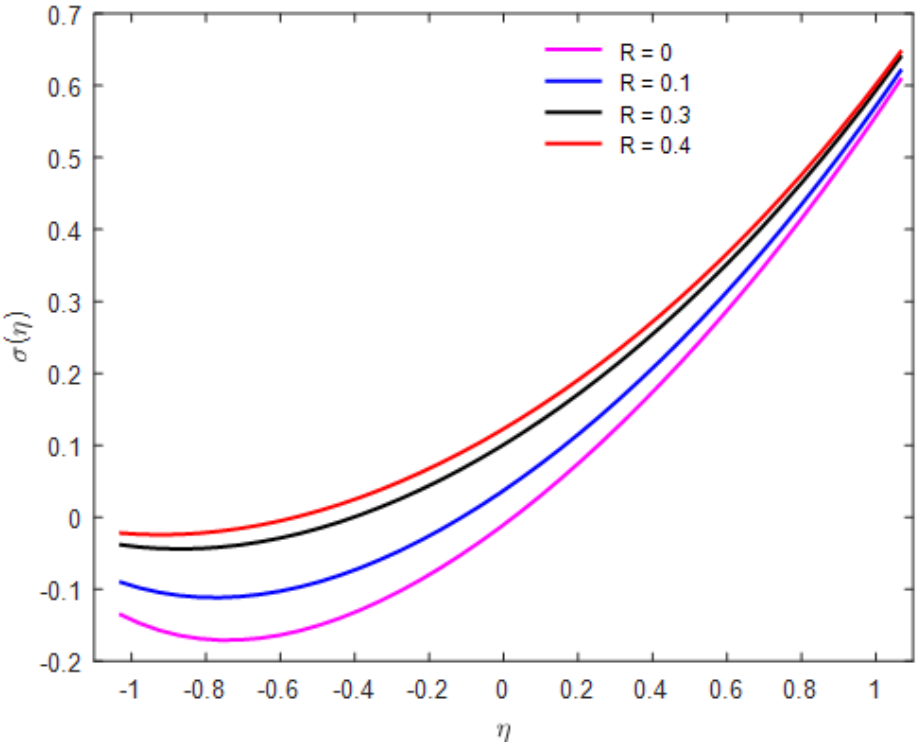

Fig.12 Variation of R on fluid concentration

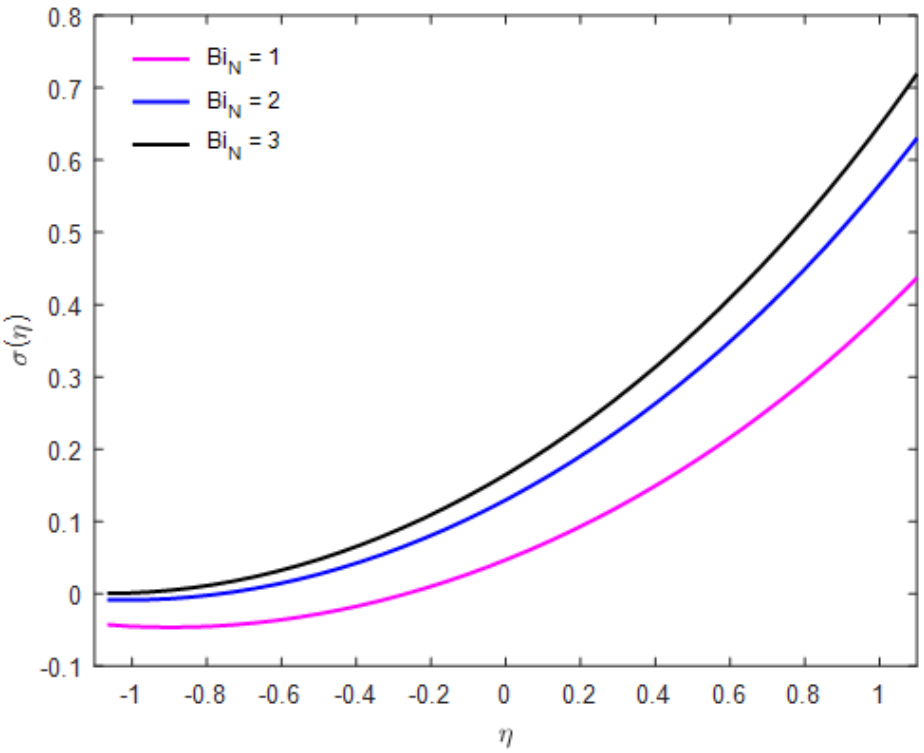

Fig.13 Variation of Bi_N on fluid concentration

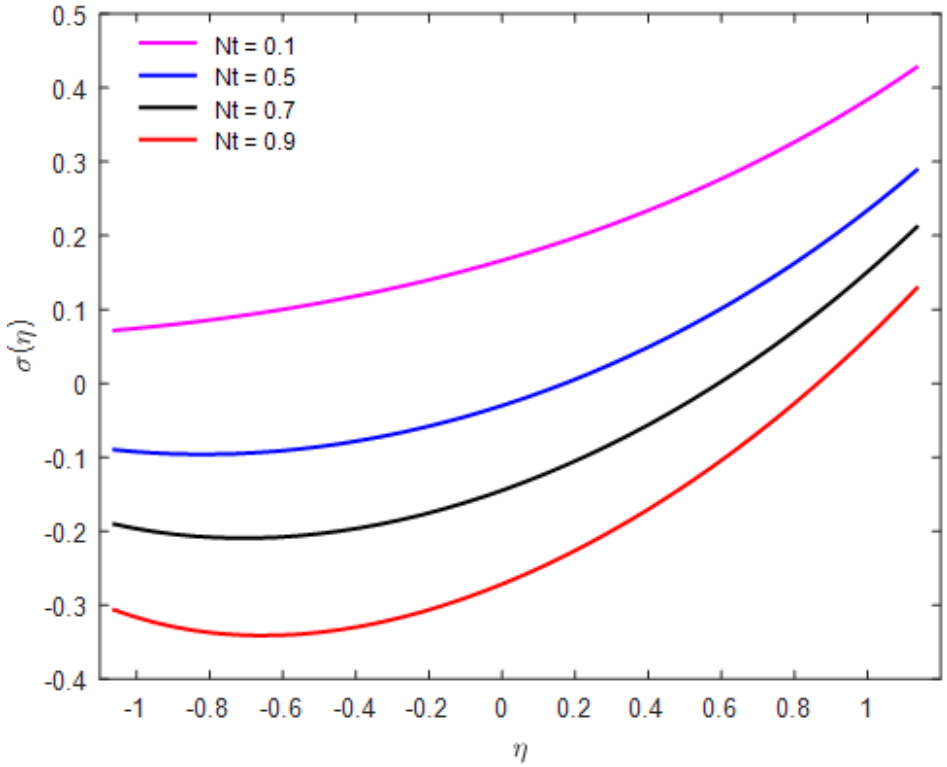

Fig.14 Variation of Nt on fluid concentration

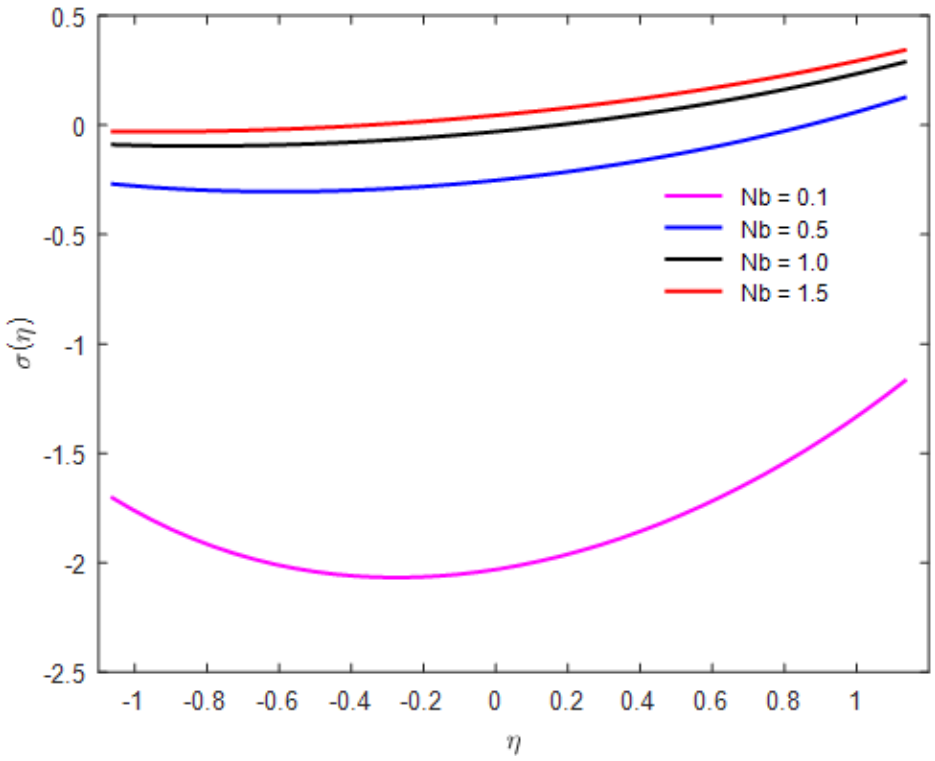

Fig.15 Variation of Nb on fluid concentration

Table-1: Variation of t on fluid regime

η	t	$\psi(\eta)$	$\psi'(\eta)$	t	$\psi(\eta)$	$\psi'(\eta)$	t	$\psi(\eta)$	$\psi'(\eta)$
-1	0	-1.5	0	0.1	-1.4851	0	0.2	-1.4703	0
-0.7333	0	-1.3942	0.7523	0.1	-1.3804	0.7446	0.2	-1.3667	0.737
-0.4667	0	-1.1185	1.2816	0.1	-1.1075	1.2686	0.2	-1.0966	1.2557
-0.2	0	-0.7273	1.6235	0.1	-0.7202	1.6071	0.2	-0.7133	1.5908
0.0667	0	-0.2674	1.7992	0.1	-0.265	1.7812	0.2	-0.2626	1.7633
0.2	0	-0.0251	1.8278	0.1	-0.0251	1.8095	0.2	-0.0251	1.7915
0.3333	0	0.2183	1.8169	0.1	0.2159	1.7988	0.2	0.2135	1.781
0.6	0	0.6872	1.6718	0.1	0.6801	1.6554	0.2	0.6732	1.6391
0.8667	0	1.0939	1.3458	0.1	1.0828	1.3327	0.2	1.0719	1.3198
1.1333	0	1.386	0.8056	0.1	1.3721	0.7979	0.2	1.3584	0.7902
1.4	0	1.5	0	0.1	1.4851	0	0.2	1.4703	0

CONFLICT OF INTERESTS

The authors declare that there is no conflict of interests.

REFERENCES

[1] T.W. Latham, Fluid motion in a peristaltic pump, MS Thesis, MIT, USA, 1966.

[2] M. Elshahed, M.H. Haroun, Peristaltic transport of Johnson–Segalman fluid under effect of a magnetic field, Math. Probl. Eng. 6 (2005), 663–677.

[3] E.F. Elshehawey, N.T. Eldabe, E.M. Elghazy, A. Ebaid, Peristaltic transport in an asymmetric channel through a porous medium, App. Math. Comput. 182 (2006), 140–150.

[4] T. Hayat, N. Ali, Perista1ltically induced motion of a MHD third grade fluid in a deformable tube, Physica A, 370 (2006), 225–239.

[5] Makinde, P.Y. Mhone, Hydromagnetic effects on internal flow separation in a diverging channel, Rom. J. Phys. 51 (2006), 959-966.

[6] Makinde, P.Y. Mhone, Heat transfer to MHD oscillatory flow in a channel filled with porous medium, Rom. J. Phys. 50 (2005), 931-938.

[7] Makinde, Collapsible tube flow-A mathematical model, Rom. J. Phys. 50 (2005), 493-506.

[8] Makinde, Asymptotic approximations for oscillatory flow in a tube of varying cross-section with permeable isothermal wall, Rom. J. Phys. 52 (2007), 59-72.

[9] B. C. Sarkar, S. Das, R.N. Jana, O.D. Makinde, Magnetohydrodynamic peristaltic flow on nanofluids in a convectively heated vertical asymmetric channel in the presence of thermal radiation, J. Nanofluids, 4 (2015), 461-473.

[10] T. Hayat, M.U. Qureshi, N. Ali, The influence of slip on the peristaltic motion of a third order fluid in an asymmetric channel, Phys. Lett. A, 372 (2008), 2653 -2664.

[11] Abd El Hakeem, Abd El Naby, AEM El Misery, F.M. Abd El Kareem, Effects of magnetic field on trapping through peristaltic motion for generalized Newtonian fluid in channel, Physica A, 367 (2006), 79 – 92.

[12] M. Kothandapani, S. Srinivas, Nonlinear peristaltic transport of a Newtonian fluid in an inclined asymmetric channel through a porous medium, Phys. Lett. A, 372 (2008), 1265–1276.

[13] S. Srinivas, M. Kothandapani, Peristaltic transport in an asymmetric channel with heat transfer – a note, Int. Commun. Heat Mass Transfer, 35 (2008), 514–522.

[14] S.U.S. Choi, Enhancing thermal conductivity of fluids with nanoparticles, in: The Proceedings of the 1995 ASME International Mechanical Engineering Congress and Exposition, San Francisco, USA, ASME, FED 231/MD 66, 1995, pp. 99–105.

[15] A.V. kuznetsov, D.A. Nield, Natural convective boundary-layer flow of a nanofluid past a vertical plate, Int. J. Therm. Sci. 49 (2010), 243–247.

[16] V. Trisaksri, S. Wongwises, Critical review of heat transfer characteristics of nanofluids, Renew. Sustain. Energy Rev. 11 (2007), 512–523.

[17] C. Kleinstreuer, Y. Feng, Experimental and theoretical studies of nanofluid thermal conductivity enhancement: a review, Nanoscale Res. Lett. 6 (2011), 229.

[18] J. Buongiorno, W. Hu, Nanofluid coolants for advanced nuclear power plants. Paper no. 5705, in: Proceedings of ICAPP ’05, Seoul, May (2005), 15–19.

[19] J. Buongiorno, Convective Transport in Nanofluids, J. Heat Transfer. 128 (2006), 240–250.

[20] L. Shi, Y. He, X. Wang, Thermophysical properties of Fe3O4@CNT nanofluid and controllable heat transfer performance under magnetic field, Energy Convers. Manage. 177 (2018), 249–257.

[21] A. Karimipour, M.H. Esfe, M.R. Safaei, D.T. Semiromi, S. Jafari, S.N. Kazi, Mixed convection of copper–water nanofluid in a shallow inclined lid driven cavity using the lattice Boltzmann method, Phys. Stat. Mech. Appl. 402 (2014), 150–168.

[22] W.A. Khan, I. Pop, Boundary-layer flows of a nanofluid past a stretching sheet, Int. J. Heat Mass Transf. 53 (2010), 2477–2483.

[23] J. Kennedy, J. Leveneur, Y. Takeda, G.V.M. Williams, S. Kupke, D.R.G. Mitchell, A. Markwitz, J.B. Metson, Evolution of the structure and magneto-optical properties of ion beam synthesized iron nanoclusters, J. Mater. Sci. 47 (3) (2012), 1127–1134.

[24] T. Prakash, G.V.M. Williams, J. Kennedy, S. Rubanov, High spin-dependent tunneling magnetoresistance in magnetite powders made by arc-discharge, J. Appl. Phys. 120 (2016), 123905.

[25] J. Leveneur, J. Kennedy, G.V.M. Williams, J. Metson, A. Markwitz, Large room temperature magnetoresistance in ion beam synthesized surface Fe nanoclusters on SiO2, Appl. Phys. Lett. 98 (2011), 053111.

[26] T. Prakash, G.V.M. Williams, J. Kennedy, P.P. Murmu, J. Leveneur, S.V. Chong, S. Rubanov, Synthesis and structural, magnetic and magnetotransport properties of permalloy powders containing nanoparticles prepared by arc discharge, J. Alloys Compounds. 608 (2014), 153–157.

[27] M.E. Borges, M. Sierra, E. Cuevas, R.D. García, P. Esparza, Photocatalysis with solar energy: sunlight-responsive photocatalyst based on TiO2 loaded on a natural material for wastewater treatment, Solar Energy, 135 (2016), 527–535.

[28] A. Zeiny, H. Jin, L. Bai, G. Lin, D. Wen, A comparative study of direct absorption nanfoluids for solar thermal applications, Solar Energy, 161 (2018), 74–82.

[29] L. Shi, Y. He, X. Wang, Y. He, Recyclable photo-thermal conversion and purification systems via Fe3O4@TiO2nanoparticles, Energy Convers. Manage. 171 (2018), 272–278.

[30] J. Prakash, E.P. Siva, D. Tripathi, S. Kuharat, O.A. Beg, Peristaltic pumping of magnetic nanofluids with thermal radiation and temperature dependent viscosity effects: modelling a solar magneto-biomimetic nanopump, Renew. Energy, 133 (2019), 1308–1326.

[31] S. Akram, S. Nadeem, A. Ghafoor, C. Lee, Consequences of nanofluid on Peristaltic flow in an asymmetric channel, Int. J. Basic Appl. Sci. 12 (2012), 75-96.

[32] H. Heidary, M.J. Kermani, Effect of nano particles on forced convection in sinusoidal wall channel, Int. Commun. Heat Mass Transf. 37 (2010), 1520–1527.

[33] N.S. Akbar, S. Nadeem, Endoscopic effects on peristaltic flow of a nanofluid, Commun. Theor. Phys. 56 (2011), 761-768.

[34] Y. Kikuchi, Effect of leukocytes and platelets on blood flow through a parallel array of microchannels: micro and micro flow relation and rheological measurer leukocyte and platelets activities, Microvascular Res. 50(1995), 288-300.

[35] J. Zueco, O. Anwar Bég, H.S. Takhar, V.R. Prasad, Thermophoretic hydromagnetic dissipative heat and mass transfer with lateral mass flux, heat source, ohmic heating and thermal conductivity effects: network simulation numerical study, Appl. Therm. Eng. 29 (2009), 2808–2815.